J. Fluid Mech. (2012), *vol.* 695, *pp.* 390–404. © Cambridge University Press 2012
doi:10.1017/jfm.2012.28

Three-dimensional instability of the flow over a forward-facing step

Daniel Lanzerstorfer and Hendrik C. Kuhlmann†

Institute of Fluid Mechanics and Heat Transfer, Vienna University of Technology, Resselgasse 3, 1040 Vienna, Austria

(Received 27 September 2011; revised 27 September 2011; accepted 10 January 2012; first published online 21 February 2012)

The global, temporal stability of the two-dimensional, incompressible flow over a forward-facing step in a plane channel is investigated numerically. The geometry is varied systematically covering constriction ratios (step-to-inlet height) from 0.23 to 0.965. A three-dimensional linear stability analysis shows that the stability boundary is a smooth continuous function of the constriction ratio. If the critical Reynolds and wavenumbers are scaled appropriately, they approach a linear asymptotic behaviour for large step heights. The critical mode is found to be stationary and confined to the region of separated flow downstream of the step for all constriction ratios. An energy-transfer analysis reveals that the basic flow becomes unstable due to a combined effect involving lift-up and flow deceleration, leading to a critical mode exhibiting steady streaks. Moreover, the receptivity of the flow to initial as well as to structural perturbations is studied by means of an adjoint analysis.

Key words: instability, transition to turbulence

1. Introduction

Flow separation and recirculation are of great interest as they play an important role in the transport and mixing of fluids. The flow over a forward-facing step in a plane channel is a prototype example for flow separation at a sharp edge near the front of a bluff body. The forward-facing-step configuration often represents the entrance geometry for polymer processes like fibre spinning, film blowing and extrusion (Chiba, Ishida & Nakamura 1995) and is important for the design of heat-transfer devices, such as combustion chambers, cooling systems and heat exchangers. Apart from its technical applications, forward-facing-step flows are also observed in rivers and lakes and might be responsible for erosional grooves (Pollard, Wakarani & Shaw 1996).

Earlier papers (see e.g. Dennis & Smith 1980; Plotkin & Mei 1986) on the forward-facing-step flow focused on the pure two-dimensional flow and on the dependence of the length of the separation zone on the Reynolds number. The topology of the two-dimensional flow is characterized by two separation zones: a first recirculation bubble ahead of the step even for low Reynolds numbers and, for larger Reynolds numbers, a second recirculation zone arises past the step which separates immediately at the sharp corner.

† Email address for correspondence: h.kuhlmann@tuwien.ac.at

https://doi.org/10.1017/jfm.2012.28 Published online by Cambridge University Press

In many experiments (Chiba *et al.* 1995; Pollard *et al.* 1996; Stüer 1999; Stüer, Gyr & Kinzelbach 1999), it was reported that the streamlines in front of the step are not closed but rather open and three dimensional in nature, which enables an entrainment into the recirculation bubble. This three-dimensionality, giving rise to the formation of streaky structures downstream of the step corner, was observed even at low Reynolds numbers. The work of Stüer *et al.* (1999) scrutinized mainly the issue of whether the separation bubble in front of the step is closed or open by studying the local three-dimensionality, but did not pay particular attention to the matter when the flow gets globally three-dimensional and consequently unstable. Nevertheless, the hydrogen bubble visualization technique revealed that the flow is turbulent at a Reynolds number of around 4800, where the Reynolds number is defined here using the entrance channel height H and the respective mean velocity $\bar{U}$.

Wilhelm, Härtel & Kleiser (2003) revealed in their direct numerical simulations that the three-dimensionality in front of the step is just a sensitive reaction of the flow to minute disturbances present in the oncoming flow. Perturbation amplitudes of less than 1 % of the mean flow, which are most likely present in the laboratory, can grow to sizeable amplitudes just ahead of the step. Moreover, it was demonstrated that there exists no significant difference between the two-dimensional and spatially averaged three-dimensional flow fields. Recently, Marino & Luchini (2009) confirmed via an adjoint analysis the findings of Wilhelm *et al.* (2003) that the flow is highly sensitive to oncoming disturbances and showed that this significant receptivity is independent from the presence of an instability. Therefore, the three-dimensionality as observed in the experiments cannot be attributed to a global instability.

Stüer (1999) investigated also numerically the flow over a forward-facing step with constriction ratios (step-to-inlet height) of $\Gamma = 0.5$ and $\Gamma = 0.25$. By a global linear stability analysis, it was shown that the critical Reynolds numbers account for $Re_c(\Gamma = 0.5) \approx 150$ and $Re_c(\Gamma = 0.25) \in [300; 400]$. The last result is in sharp conflict with the findings of Wilhelm (2000) and Wilhelm *et al.* (2003), who showed that the flow for $\Gamma = 0.25$ subjected to three-dimensional perturbations is absolutely stable for $Re = 1320$, representing a lower bound to the stability boundary. Recently, Marino & Luchini (2009) computed the stability boundaries for the constriction ratios $\Gamma = 0.5$ and $\Gamma = 0.25$. They obtained critical Reynolds numbers of $Re_c(\Gamma = 0.5) \approx 997$ and $Re_c(\Gamma = 0.25) \approx 3440$, which are approximately 10 times higher than the ones of Stüer (1999).

The present study is conducted on the one hand to clarify the discrepancy between the critical Reynolds numbers of Stüer (1999) and Marino & Luchini (2009) and on the other hand to understand the physical nature of the instability, which has never been examined for the forward-facing step problem. Hence, a global stability analysis of the two-dimensional basic flow is carried out with a systematic variation of the geometry, covering a wide range of constriction ratios from $\Gamma = 0.23$ to $\Gamma = 0.965$. It will be shown that the critical data obtained by Marino & Luchini (2009) are not fully grid independent and clearly depend on the length of the inlet channel. We find that the grid- and entrance-length-independent critical Reynolds numbers are up to 1.7 times larger than those obtained by Marino & Luchini (2009). In addition, the instability mechanism of the global modes will be elucidated by analysing the kinetic energy transferred from the basic flow to the critical mode. The prevailing work also comprises a structural sensitivity analysis in order to assess the process which leads to the self-sustained perturbations.

Section 2 deals with the methods of investigation, the problem definition, the formulation of the governing equations, the numerical methods and the code

https://doi.org/10.1017/jfm.2012.28 Published online by Cambridge University Press

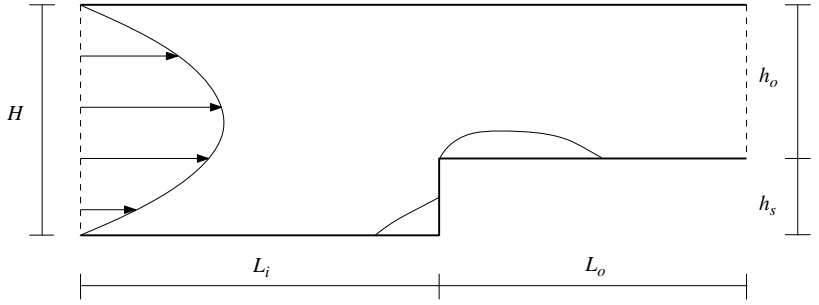


FIGURE 1. Sketch of the flow domain of the forward-facing step problem.

verification. The main part of the paper, § 3, is devoted to the results of the stability analyses, followed by a discussion of the physical mechanism. The conclusions in § 4 summarize the main results.

2. Methods of investigation

2.1. *Problem formulation*

The analysis is concerned with an incompressible flow of a Newtonian fluid over a rectangular forward-facing step in the (x, y) plane. The flow domain is assumed to be infinitely extended in the spanwise (z) direction. The geometry is depicted in figure 1, consisting of an inlet channel of height H and length L_i followed by a suddenly constricted channel of height h_o and length L_o. The origin of the coordinate system is located at the bottom of the step of height $h_s = H - h_o$.

Using the mean velocity $\bar{U}$ of the inlet flow, the height H of the inlet channel and the kinematic viscosity ν of a Newtonian fluid for the scaling, the steady, incompressible Navier–Stokes and continuity equations are given by

$$\boldsymbol{u}_0 \cdot \boldsymbol{\nabla} \boldsymbol{u}_0 = -\boldsymbol{\nabla} p_0 + \frac{1}{Re} \nabla^2 \boldsymbol{u}_0, \tag{2.1a}$$

$$\boldsymbol{\nabla} \cdot \boldsymbol{u}_0 = 0. \tag{2.1b}$$

We are interested in the ideal case in which both L_i and L_o tend to infinity. For the numerical treatment, however, both channels must be truncated. The corresponding finite lengths will be selected sufficiently large such that the flow near the step is independent of L_i and L_o. The problem is then governed only by two parameters: the Reynolds number Re and the constriction ratio Γ defined as

$$Re = \frac{H\bar{U}}{\nu} \quad \text{and} \quad \Gamma = \frac{h_s}{H}. \tag{2.2}$$

At the inlet $x = -L_i/H$, plane Poiseuille flow $u_0(y) = 6y(1 - y)$ and $v_0 = 0$ is assumed for $y \in [0; 1]$. Along the step and all channel walls, no-slip and no-penetration boundary conditions $\boldsymbol{u}_0 = 0$ are adopted. At the outlet $x = L_o/H$, homogeneous Neumann conditions $\partial_x \boldsymbol{u}_0 = 0$ are used for all velocity components, and the pressure level is specified by $p_0 = 0$.

https://doi.org/10.1017/jfm.2012.28 Published online by Cambridge University Press

2.2. *Linear stability analysis*

The equations for the linear stability of the two-dimensional basic flow $\boldsymbol{u}_0 = (u_0,\ v_0,\ 0)^{\mathrm{T}}$ take the form

$$\partial_t \tilde{\boldsymbol{u}} + \boldsymbol{u}_0 \cdot \boldsymbol{\nabla}\tilde{\boldsymbol{u}} + \tilde{\boldsymbol{u}} \cdot \boldsymbol{\nabla}\boldsymbol{u}_0 = -\boldsymbol{\nabla}\tilde{p} + \frac{1}{\mathrm{Re}}\nabla^2\tilde{\boldsymbol{u}}, \tag{2.3a}$$

$$\boldsymbol{\nabla} \cdot \tilde{\boldsymbol{u}} = 0. \tag{2.3b}$$

The boundary conditions for the perturbations $(\tilde{\boldsymbol{u}}, \tilde{p})$ are the same as for the basic flow, except at the inlet, where we prescribe $\tilde{\boldsymbol{u}} = 0$. These inflow and outflow boundary conditions are appropriate for the linear instability analysis of open systems (Theofilis 2011). Note that setting the pressure perturbation to zero at the outlet merely serves to fix the pressure perturbation level to a constant for comparison, but does not affect the results.

Since (2.3) is homogeneous in time and in the z direction, the three-dimensional perturbations can be expressed as a superposition of normal modes

$$\begin{pmatrix} \tilde{\boldsymbol{u}} \\ \tilde{p} \end{pmatrix}(x, y, z, t) = \begin{pmatrix} \hat{\boldsymbol{u}} \\ \hat{p} \end{pmatrix}(x, y)\mathrm{e}^{-\gamma t + \mathrm{i}kz} + \mathrm{c.c.}, \tag{2.4}$$

where k is a real, positive and continuous wavenumber in the spanwise direction. The term $\gamma = \sigma + \mathrm{i}\omega$ represents the real decay rate σ and the oscillation frequency ω. $\hat{\boldsymbol{u}}$ and $\hat{p}$ constitute the complex amplitude/shape functions of the perturbations.

Substitution of the ansatz (2.4) into the perturbation (2.3) yields a complex, generalized and singular eigenvalue problem. Following the ideas of Theofilis (2003), it is possible to deduce a real eigenvalue problem as the base flow $\boldsymbol{u}_0 = (u_0,\ v_0,\ 0)^{\mathrm{T}}$ is two dimensional. Redefining the spanwise component $\hat{w}$ by $\mathrm{i}\hat{w}$ converts the complex eigenvalue problem into a real one:

$$\boldsymbol{A} \cdot \boldsymbol{x} = \gamma \boldsymbol{B} \cdot \boldsymbol{x}, \tag{2.5}$$

where $\boldsymbol{x} = (\hat{u},\ \hat{v},\ \hat{w},\ \hat{p})^{\mathrm{T}}$ and $\boldsymbol{A}$ and $\boldsymbol{B}$ are linear and real operators.

The critical Reynolds number Re_c is determined by the condition that the minimum possible real decay rate σ vanishes over all discrete modes and continuous wavenumbers for a given geometry characterized by Γ.

2.3. *Energy analysis*

For a discussion of the physical instability mechanism, the kinetic energy transferred between the basic flow and the critical perturbation mode is calculated. The rate of change of the kinetic energy $\mathrm{d}E_{\mathrm{kin}}/\mathrm{d}t$ is given by the Reynolds–Orr equation

$$\frac{1}{D}\frac{\mathrm{d}E_{\mathrm{kin}}}{\mathrm{d}t} = -1 + \sum_{i=1}^{4}\int_V I_i' \,\mathrm{d}V - \frac{1}{2}\int_{S_o} I_5 \,\mathrm{d}S, \tag{2.6}$$

where V is the volume and S_o the outlet surface, both for one period of the normal mode. The energy-transfer rates are normalized by the total dissipation rate

$$D = \frac{1}{2Re}\int_V \left[\boldsymbol{\nabla}\tilde{\boldsymbol{u}} + (\boldsymbol{\nabla}\tilde{\boldsymbol{u}})^{\mathrm{T}}\right] : \left[\boldsymbol{\nabla}\tilde{\boldsymbol{u}} + (\boldsymbol{\nabla}\tilde{\boldsymbol{u}})^{\mathrm{T}}\right] \mathrm{d}V. \tag{2.7}$$

The surface integral at the outlet

$$-\frac{1}{2}\int_{S_o} I_5 \,\mathrm{d}S = -\frac{1}{2}\int_{S_o} \frac{\tilde{\boldsymbol{u}}^2 u_0}{D}\,\mathrm{d}S \tag{2.8}$$

https://doi.org/10.1017/jfm.2012.28 Published online by Cambridge University Press

represents the kinetic perturbation energy which is convected out of the domain by the basic flow resulting from the term $-\tilde{\boldsymbol{u}} \cdot (\boldsymbol{u}_0 \cdot \boldsymbol{\nabla}\tilde{\boldsymbol{u}})$. Moreover, no work is done by the pressure as we assume $\tilde{p} = 0$ at the outlet.

Decomposing the perturbation field into components parallel and perpendicular to the basic flow $\boldsymbol{u}_0$,

$$\tilde{\boldsymbol{u}}_\parallel = \frac{(\tilde{\boldsymbol{u}} \cdot \boldsymbol{u}_0)\boldsymbol{u}_0}{\boldsymbol{u}_0 \cdot \boldsymbol{u}_0}, \quad \tilde{\boldsymbol{u}}_\perp = \tilde{\boldsymbol{u}} - \tilde{\boldsymbol{u}}_\parallel, \tag{2.9}$$

the local normalized energy-transfer terms in streamline coordinates read

$$\sum_{i=1}^{4} I_i' = -\frac{1}{D}\left[\tilde{\boldsymbol{u}}_\perp \cdot (\tilde{\boldsymbol{u}}_\perp \cdot \boldsymbol{\nabla}\boldsymbol{u}_0) + \tilde{\boldsymbol{u}}_\parallel \cdot (\tilde{\boldsymbol{u}}_\perp \cdot \boldsymbol{\nabla}\boldsymbol{u}_0) + \tilde{\boldsymbol{u}}_\perp \cdot (\tilde{\boldsymbol{u}}_\parallel \cdot \boldsymbol{\nabla}\boldsymbol{u}_0) + \tilde{\boldsymbol{u}}_\parallel \cdot (\tilde{\boldsymbol{u}}_\parallel \cdot \boldsymbol{\nabla}\boldsymbol{u}_0)\right], \tag{2.10}$$

where all summands I_i' are numbered consecutively.

2.4. *Adjoint analysis*

The adjoint perturbation problem is defined as

$$-\partial_t \tilde{\mathfrak{u}} - \boldsymbol{u}_0 \cdot \boldsymbol{\nabla}\tilde{\mathfrak{u}} + \tilde{\mathfrak{u}} \cdot (\boldsymbol{\nabla}\boldsymbol{u}_0)^{\mathrm{T}} = -\boldsymbol{\nabla}\tilde{\mathfrak{p}} + \frac{1}{\mathrm{Re}}\nabla^2\tilde{\mathfrak{u}}, \tag{2.11a}$$

$$\boldsymbol{\nabla} \cdot \tilde{\mathfrak{u}} = 0, \tag{2.11b}$$

with the adjoint normal mode ansatz

$$\begin{pmatrix} \tilde{\mathfrak{u}} \\ \tilde{\mathfrak{p}} \end{pmatrix}(x, y, z, t) = \begin{pmatrix} \hat{\mathfrak{u}} \\ \hat{\mathfrak{p}} \end{pmatrix}(x, y)\, \mathrm{e}^{\bar{\gamma}t + \mathrm{i}kz} + c.c. \tag{2.12}$$

As the adjoint system is only well posed in the negative time direction, it is sometimes referred to as the backward system. Since the operators of the eigenvalue problem (2.5) are real and linear, the adjoint modes can be easily computed by taking the transpose of these operators:

$$\boldsymbol{A}^{\mathrm{T}} \cdot \boldsymbol{\mathfrak{X}} = \bar{\gamma}\, \boldsymbol{B}^{\mathrm{T}} \cdot \boldsymbol{\mathfrak{X}} \tag{2.13}$$

with $\boldsymbol{\mathfrak{X}} = (\hat{\mathfrak{u}}, \hat{\mathfrak{v}}, \hat{\mathfrak{w}}, \hat{\mathfrak{p}})^{\mathrm{T}}$, where the correct boundary conditions for the adjoint fields are automatically taken into account. The direct and adjoint eigenvectors are normalized by imposing the conditions

$$\|\hat{\boldsymbol{u}}\| := \sqrt{\langle \hat{\boldsymbol{u}}, \hat{\boldsymbol{u}} \rangle}, \quad \int_{\mathscr{D}} \hat{\boldsymbol{u}} \cdot \hat{\boldsymbol{u}}\, \mathrm{d}\mathscr{D} = 1, \tag{2.14a}$$

$$\langle \hat{\mathfrak{u}}, \hat{\boldsymbol{u}} \rangle = \int_{\mathscr{D}} \hat{\mathfrak{u}} \cdot \hat{\boldsymbol{u}}\, \mathrm{d}\mathscr{D} = 1 \tag{2.14b}$$

over the computational domain $\mathscr{D}$. Note that the adjoint eigenvector is not scaled according to the naturally defined norm based upon the inner product of the space itself $\|\hat{\mathfrak{u}}\|$, because the normalization (2.14*b*) simplifies (2.16).

The adjoint velocity fields $|\hat{\mathfrak{u}}| = |(\hat{\mathfrak{u}}, \hat{\mathfrak{v}}, \hat{\mathfrak{w}})^{\mathrm{T}}|$ contain information about the flow sensitivity to initial conditions and to momentum forcing. Moreover, an adjoint analysis allows us to identify the sensitivity of the eigenvalue spectrum to spatially localized perturbations. Giannetti & Luchini (2007) have shown that the drift $\Delta\gamma$

https://doi.org/10.1017/jfm.2012.28 Published online by Cambridge University Press

due to a perturbation localized at (x_0, y_0) of the eigenvalue γ associated with the eigenvector $\hat{\boldsymbol{u}}$ is bounded by

$$|\Delta\gamma| \leqslant c\Upsilon(x_0, y_0) \tag{2.15}$$

with

$$\Upsilon(x, y) = \frac{|\hat{\boldsymbol{u}}(x, y)|\,|\hat{\mathbf{u}}(x, y)|}{\underbrace{\langle\hat{\mathbf{u}}, \hat{\boldsymbol{u}}\rangle}_{=1}}, \tag{2.16}$$

where $c > 0$ of (2.15) is a measure for the strength of the localized forcing. Hence, the scaled product $\Upsilon(x, y)$ between the direct and adjoint velocity eigenmodes represents a measure for the sensitivity of the temporal growth rates to local perturbations.

2.5. *Numerical methods and code verification*

The numerical approach is identical to the one of Lanzerstorfer & Kuhlmann (2011), where details and references can be found. In short, the primitive variables are discretized on a staggered grid using a finite-volume method of second order. For the basic flow, the nonlinear set of equations (2.1) is solved with Newton's method. The grid is systematically refined towards the walls and around the step. Neighbouring cells are not allowed to differ by more than 3 % in width.

The linear stability equations (2.3) are discretized on the same grid where the spanwise component of the perturbation field $\tilde{w}$ resides with the pressure nodes. Inserting the normal mode ansatz (2.4) into (2.3) results in a complex, generalized and singular eigenvalue problem which is transformed into a real one. For determining the critical Reynolds number, a shift–invert transformation with zero shift is applied first, which gives the eigenvalues with smallest magnitude. In a second step a Cayley transformation is adopted to ensure that the eigenvalues with smallest real part are detected. All eigenvalue problems are solved with an implicitly restarted Arnoldi algorithm with a Krylov subspace dimension of 200.

The numerical code has been verified thoroughly in Lanzerstorfer & Kuhlmann (2011) by computing the critical Tollmien–Schlichting wave for plane-channel flow, by checking the critical Reynolds and wavenumbers against the results of Theofilis (2000) and Albensoeder, Kuhlmann & Rath (2001) for the lid-driven square-cavity problem and by comparing the critical values for the backward-facing step problem with those obtained by Barkley, Gomes & Henderson (2002). To give further credence to the present numerical code, the critical data for the forward-facing step flow are computed for the same geometrical parameters as Marino & Luchini (2009). Using $L_i = 1H$ and $L_o(\Gamma = 0.5) = 6h_o$ or $L_o(\Gamma = 0.25) = 5.\dot{3}h_o$, we obtain $Re_c = 1037.8\,(997)$ and $k_c = 6.0975\,(6.2)$ for $\Gamma = 0.5$ and $Re_c = 3469.7\,(3440)$ and $k_c = 5.9124\,(6.4)$ for $\Gamma = 0.25$, where the values of Marino & Luchini (2009) are given in parentheses. Both sets of data agree well. However, as can be noticed, the results of the above-mentioned authors are not fully grid converged.

Grid convergence was obtained by using the minimum grid resolution of $\Delta x_{\min} = \Delta y_{\min} = 10^{-3}$ (in units of H) along the walls and around the step. The cell width is increased smoothly using a stretching factor of 1.03 until the maximum grid spacings $\Delta x_{\max} = 0.02$ and $\Delta y_{\max} = 0.01$ are reached. The number of grid points used are shown in table 2 for representative constriction ratios. N_x^i and N_y^i represent the numbers of grid points in the x and y directions, respectively, in the inflow channel while N_x^o and N_y^o are the numbers of grid points in the outflow channel.

https://doi.org/10.1017/jfm.2012.28 Published online by Cambridge University Press

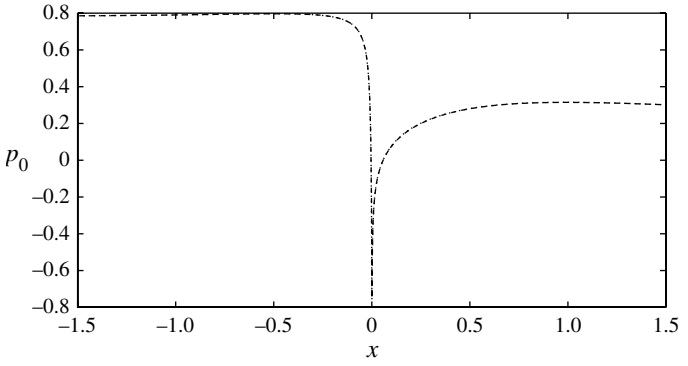


FIGURE 2. Pressure distribution at $y = 0.2505$ for $Re = 1320$ in the vicinity of the step corner for $\Gamma = 0.25$. Dashed lines depict the present result and dotted curves the solution of ANSYS FLUENT 13.0.

As a final verification, the pressure distribution is compared to the one obtained by ANSYS FLUENT 13.0. The grid is built with the same number of grid points and the same grid resolution where a hyperbolic tangent stretching function is used to distribute the grid points. The pressure and the gradients are resolved with methods of second order and for the convective terms the QUICK scheme is applied. In figure 2 the pressure distribution for $\Gamma = 0.25$ is shown slightly above the step at $y = 0.2505$ for $Re = 1320$. Dashed lines represent the present solution and dotted ones the result of ANSYS FLUENT 13.0. Both curves are indistinguishable on the scale shown. The pressure has steep gradients in the vicinity of the step due to the corner singularity and features a minimum of -0.7532 at $x = 0.0005$ with the present code. ANSYS FLUENT 13.0 yields a minimum of -0.7519, where the pressure level is set to zero at the outlet.

3. Results

3.1. *Parameter dependence*

To obtain critical Reynolds and wavenumbers for infinitely long in- and outlet channels, the influence of L_i and L_o on Re_c and k_c was studied. The length of the entrance channel L_i turns out to be of utmost importance. If the inflow channel is too short, the basic flow in the vicinity of the step is not fully developed to the basic flow for $L_i \to \infty$. This is shown in figure 3, where the basic flow is depicted for $L_i = 8H$ and $L_i = 1H$ for $Re = 3518.4$ and $\Gamma = 0.25$, using the same outflow channel length $L_o = 32h_o$. It can be seen that for $L_i = 1H$ the length of the first separation bubble is too short and the one of the secondary vortex is too long.

Its effect on the stability boundaries is shown in table 1. Results are given for $\Gamma \in \{0.25,\ 0.5,\ 0.75\}$, but a similar convergence of the critical data, as L_i is increased, is obtained for all constriction ratios covered here. As can be seen from table 1, the length of the inlet channel should be at least $L_i = 6H$ to restrict the inlet-channel-length effect on Re_c to below $\approx 0.03\,\%$.

The influence of the outlet-channel length L_o on the stability boundaries was also scrutinized (not shown here). We found that $L_o = 32h_o$ was more than sufficient to keep the effect on Re_c and k_c below $\approx 0.01\,\%$. Figure 4 shows for $\Gamma = 0.5$, $Re = 1423.9$ and $L_i = 8H$ the basic velocity profiles $u_0(y)$ at the outlet for two

https://doi.org/10.1017/jfm.2012.28 Published online by Cambridge University Press

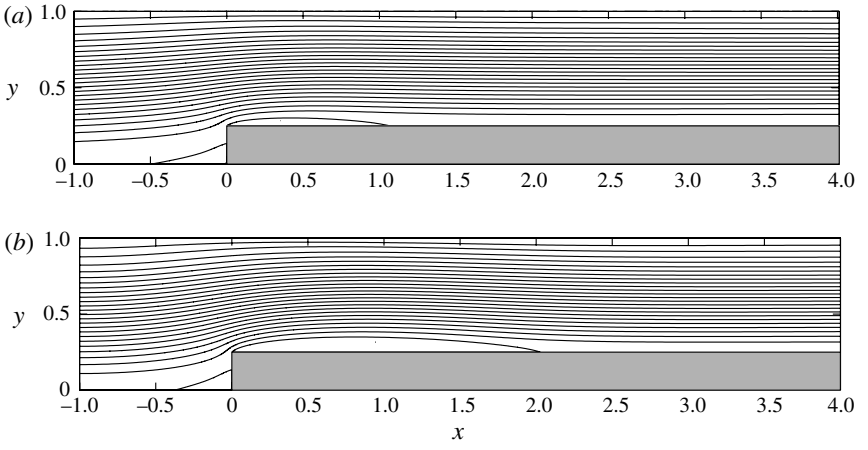


FIGURE 3. Streamlines of the base flow for $\Gamma = 0.25$, $Re = 3518.4$ and $L_o = 32h_o$ for different inflow channel lengths: (*a*) $L_i = 8H$ and (*b*) $L_i = 1H$.

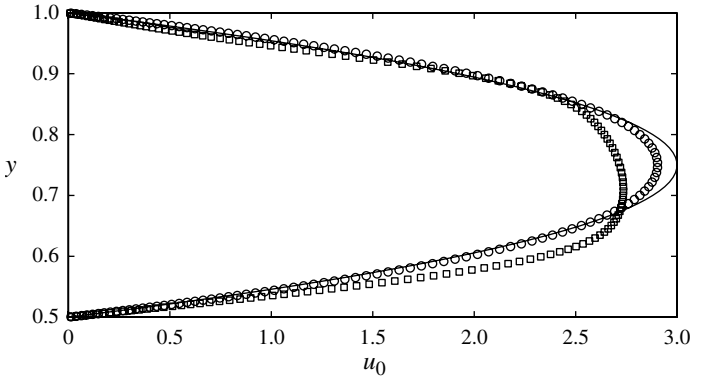


FIGURE 4. Velocity profiles $u_0(y)$ at the outlet for $\Gamma = 0.5$, $Re = 1423.9$ and $L_i = 8H$ shown for $L_o = 6h_o$ (squares) and for $L_o = 32h_o$ (dots). The solid line represents the fully developed plane Poiseuille flow.

L_i	$1H$	$2H$	$3H$	$6H$	$8H$	$12H$	Γ
Re_c	3518.4	5290.6	5741.9	5886.7	5888.4	5888.4	0.25
k_c	5.9424	7.2459	7.6341	7.7601	7.7621	7.7622	0.25
Re_c	1048.1	1366.5	1413.1	1423.8	1423.9	1423.9	0.5
k_c	6.1240	6.7581	6.8615	6.8831	6.8833	6.8833	0.5
Re_c	771.89	843.16	846.89	848.50	848.51	848.51	0.75
k_c	11.075	11.459	11.4998	11.507	11.508	11.508	0.75

TABLE 1. Critical values Re_c and k_c as functions of the entrance length L_i for multiples of the characteristic length scale H for three different constriction ratios and $L_o = 32h_o$.

different outflow channel lengths, $L_o = 32h_o$ and $L_o = 6h_o$ (the choice of Marino & Luchini 2009). It can be noticed that the velocity profile for $L_o = 6h_o$ deviates substantially from the fully developed plane Poiseuille flow; it is not even symmetrical.

https://doi.org/10.1017/jfm.2012.28 Published online by Cambridge University Press

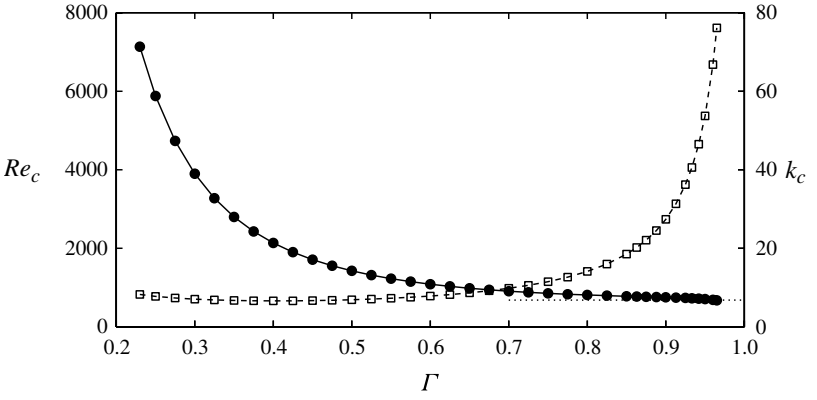


FIGURE 5. Critical Reynolds number Re_c (dots and full line) and wavenumber k_c (squares and dashed line) as functions of the constriction ratio Γ. The dotted line represents the extrapolated value for $\Gamma \to 1$ with $Re_c \approx 680$.

Γ	Re_c	k_c	N_y^i	N_y^o	N_x^o	Γ	Re_c	k_c	N_y^i	N_y^o	N_x^o
0.23	7135.0	8.2324	276	174	1314	0.6	1083.3	7.8358	288	132	716
0.25	5888.4	7.7621	278	172	1282	0.7	904.41	9.8126	282	116	554
0.3	3902.6	7.0462	282	166	1201	0.8	807.38	14.120	270	94	393
0.4	2135.4	6.6002	288	156	1039	0.9	751.02	27.434	248	62	231
0.5	1423.9	6.8833	292	146	878	0.95	706.21	53.838	228	38	150

TABLE 2. Critical data for selected constriction ratios Γ. The number of grid points (N_x, N_y) in the (x, y) plane is also given. For all calculations $N_x^i = 473$ is used.

To sum up, all results reported in the present study are calculated with an entrance length of $L_i = 8H$ and an outflow length of $L_o = 32h_o$ to minimize deviations from the asymptotic limit $(L_i, L_o) \to \infty$. For this configuration and using more than twice the number of grid points in the y direction as Marino & Luchini (2009), we obtain stability boundaries up to 70 % higher than the ones of these authors.

3.2. *Stability boundaries*

Representative numerical critical Reynolds and wavenumbers are collected in table 2 for selected expansion ratios. Also, the number of grid points used is indicated.

Figure 5 shows critical values as functions of the constriction ratio Γ. The stability boundary varies smoothly with the constriction ratio. All critical modes are stationary. The smallest constriction ratio considered was $\Gamma = 0.23$ with a critical Reynolds number of $Re_c = 7135$. This Reynolds number is below the critical condition of the plane Poiseuille flow, which is around $Re_c^{PPF} \approx 7700$ for the present scaling. For larger constriction ratios (increasing step heights) Re_c decreases continuously and seems to approach an asymptotic limit $Re_c \approx 680$ for $\Gamma \to 1$.

In the limit $\Gamma \to 1$, the height of the outlet channel h_o remains the only geometrical length scale. The correspondingly defined Reynolds and wavenumbers are, respectively,

$$Re^* = Re\frac{h_o}{H}, \quad k^* = k\frac{h_o}{H} \quad \text{for } \Gamma \in [0.5; \to 1[. \tag{3.1}$$

https://doi.org/10.1017/jfm.2012.28 Published online by Cambridge University Press

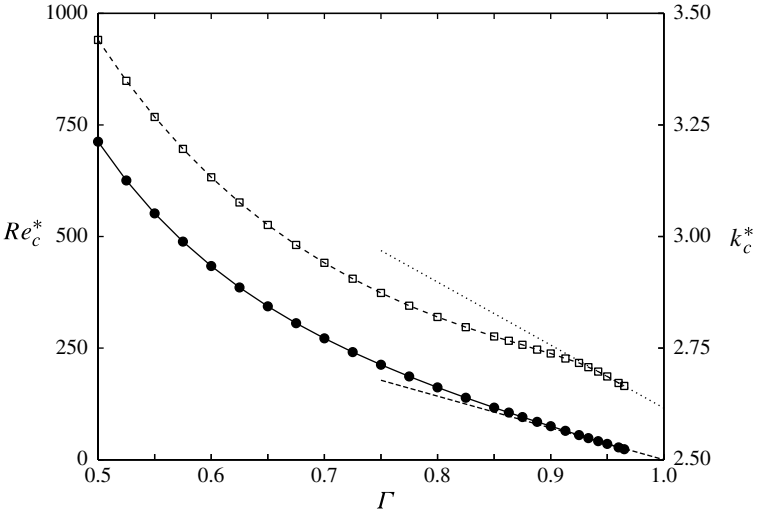


FIGURE 6. Critical Reynolds number Re_c^* (dots and full line) and wavenumber k_c^* (squares and dashed line) as functions of the constriction ratio Γ. The data are scaled according to (3.1). The dash-dotted and dotted lines represent the best estimate for an asymptotic behaviour for $\Gamma \to 1$ as mentioned in the text.

Using the above scaling, the critical data are depicted in figure 6. The critical Reynolds number suggests a linear asymptotic scaling as $\Gamma \to 1$. The linear scaling is estimated by a linear fit through the three discrete data points for the largest values of Γ, resulting in $Re_c^* \approx 711.94(1 - \Gamma)$. A linear scaling of k_c^* for $\Gamma \to 1$ is not as obvious. Nevertheless, the dotted line in figure 6, being obtained in the same way as for Re_c^*, corresponds to $k_c^* \approx 4.0272–1.4115\Gamma$.

Regardless of the constriction ratio Γ, the two-dimensional basic flow over a forward-facing step features a region of separated flow in the 90° corner in front of the step. We shall call this vortex the primary vortex, as it is the first one to appear as Re is increased. For higher Reynolds numbers, a secondary recirculation bubble arises which separates immediately downstream of the sharp corner of the step. We find that this secondary vortex is of key importance for the flow instability, as the critical modes and their associated energy-production rates are most pronounced near this region. Therefore, we shall discuss the flow characteristics near the secondary vortex, although the computational domain is much more extended in the x direction.

3.3. *Instability by lift-up and flow deceleration*

We find that the physical instability mechanism is independent of the constriction ratio. As a representative case, we discuss the instability for $\Gamma = 0.25$, because this constriction ratio was also analysed by Wilhelm *et al.* (2003). For this purpose, it proved useful to compute the kinetic energy transfer rates between the basic and the perturbation flows. The normalized energy-production rates in streamline coordinates I' integrated over the whole flow domain are summarized in table 3 for $\Gamma = 0.25$. Note that all normalized energy-production terms sum up to unity with accuracy better than 10^{-4}.

The critical mode at $Re_c = 5888.4$ and $k_c = 7.7621$ is confined to the region of the secondary separation bubble, which arises for $Re \gtrsim 770$ if $\Gamma = 0.25$. From figure 7(*a*), it can be seen that the disturbances gain most of the energy in the shear layer

https://doi.org/10.1017/jfm.2012.28 Published online by Cambridge University Press

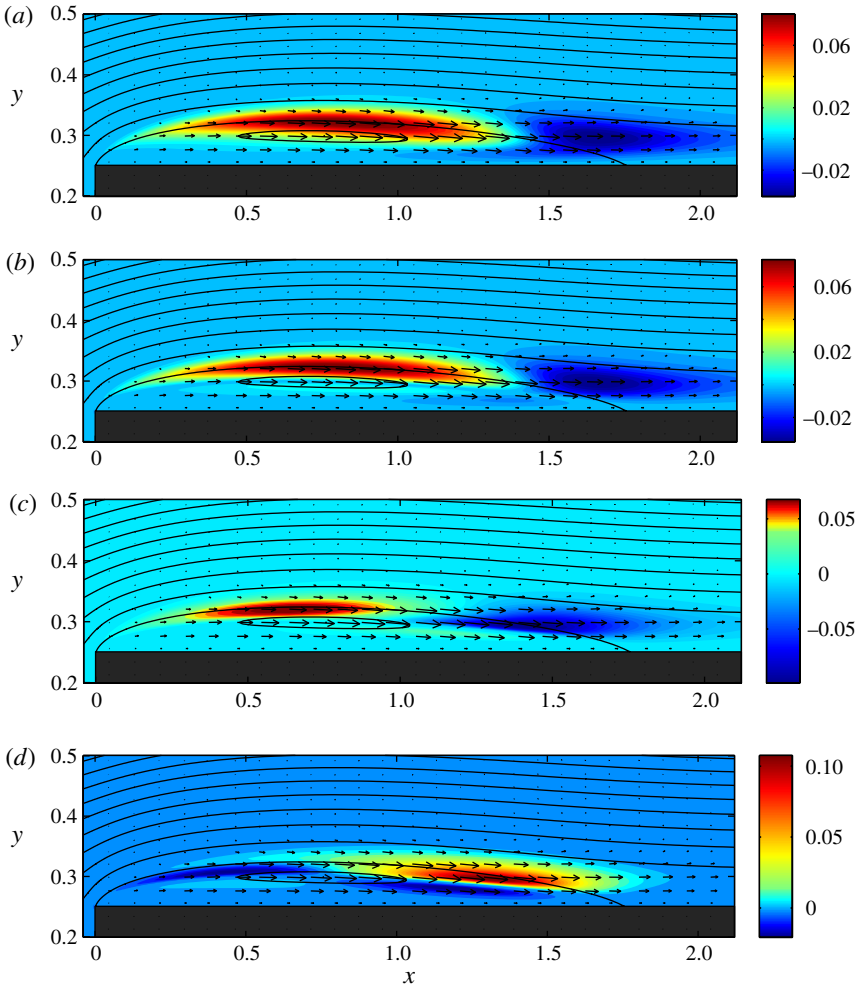


FIGURE 7. Critical velocity fields (arrows) and local energy-production rates for $\Gamma = 0.25$ in a plane $z = 0$ in which all production terms shown exhibit their local extrema: (*a*) total local production $\sum_i I_i$, (*b*) $I_2' + I_4'$, (*c*) I_2' and (*d*) I_4'. The y axes are stretched by a factor of two.

i	1	2	3	4	$\int_{S_o} I_5 \,\mathrm{d}S$
$\int_V I_i' \,\mathrm{d}V$	0.0508	0.2166	0.0869	0.7246	−0.0788
$\int_V \lvert I_i' \rvert \,\mathrm{d}V$	0.1211	0.5404	0.0879	0.2506	

TABLE 3. Global normalized energy-production rates for $\Gamma = 0.25$.

around the separating streamline. The critical mode appears as slow and fast streaks alternating in the spanwise direction, which are shown in figure 8 for two periods $2\lambda_c = 4\pi/k_c$. The critical wavelength is approximately three times the step height, which agrees well with the findings of Wilhelm *et al.* (2003) and the observations in the experiments of Stüer *et al.* (1999).

https://doi.org/10.1017/jfm.2012.28 Published online by Cambridge University Press

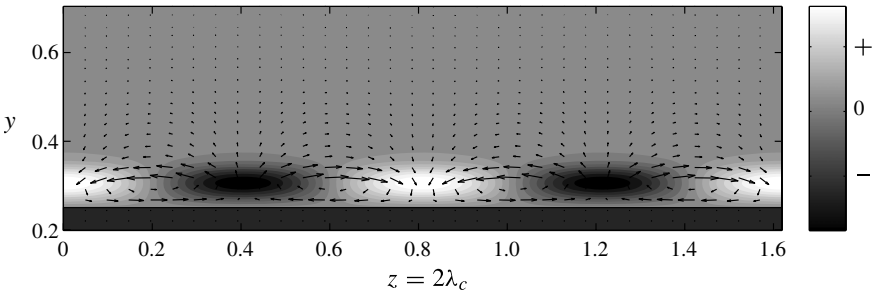


FIGURE 8. Critical velocity fields (arrows) and streamwise perturbation velocity $\tilde{u}$ (colour) for $\Gamma = 0.25$ at $x = 0.8342$, where the energy production features its local maximum.

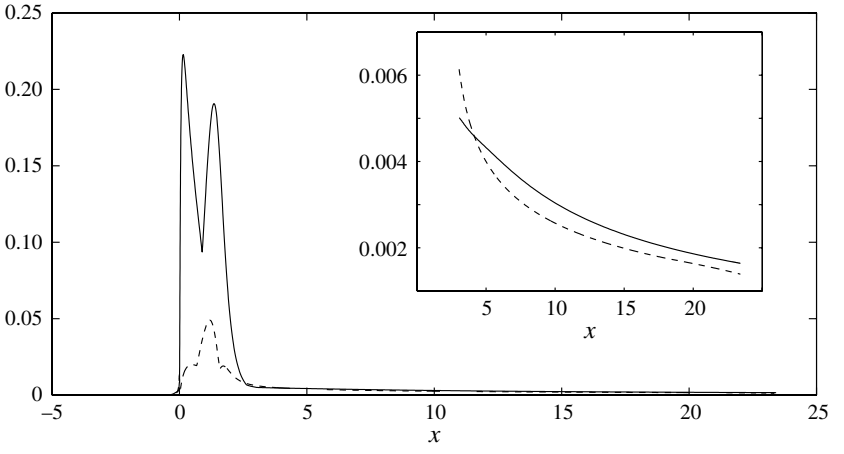


FIGURE 9. Relative magnitude of the streamwise vortices expressed by $\max_y |\hat{v}(x, y)|$ (dashed) and $\max_y |\hat{w}(x, y)|$ as functions of the streamwise coordinate x for $\Gamma = 0.25$ at $Re_c = 5888.4$. The inset shows the decay of the amplitudes for $x \in [3; 24]$.

The streaky structure can be explained by the classical lift-up mechanism (Landahl 1975, 1980). This effect generates large-amplitude velocity perturbations in the streamwise direction by the weak lift-up of fluid particles in wall-normal direction in the presence of a strong shear flow. Figure 7(*a–d*) indicate that the streamwise perturbation velocity $\tilde{u}$ clearly prevails over the wall-normal component $\tilde{v}$. The streamwise vortices creating the streaks are clearly localized in the immediate vicinity of the step. This is confirmed in figure 9, which shows the maximum over y of the absolute amplitudes $|\hat{v}(x, y)|$ and $|\hat{w}(x, y)|$. The amplitudes are continuously decaying in the streamwise direction, which is shown in the inset of figure 9 for $x \in [3; 24]$.

Schmid & Henningson (2001) demonstrated that the lift-up mechanism can give rise to transient growth for parallel shear flows. By contrast, the disturbances are self-sustained here on account of the feedback provided by the secondary recirculating bubble. I'_4 represents the largest destabilizing factor in the integral energy budget which describes an amplification process due to basic flow deceleration (cf. table 3). However, its importance is qualified because I'_2 is strongly stabilizing in the same region where I'_4 features its maximum production (figure 7*c,d*). By integrating over the absolute value of the local energy production rates $\int_V |I'_i| \, \mathrm{d}V$, one can see that the

https://doi.org/10.1017/jfm.2012.28 Published online by Cambridge University Press

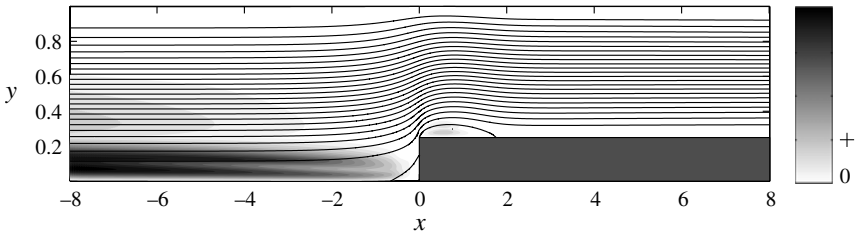


FIGURE 10. Receptivity to initial conditions and momentum forcing $|\hat{\mathbf{u}}|$ for the most dangerous mode for $\Gamma = 0.25$ at $Re_c = 5888.4$.

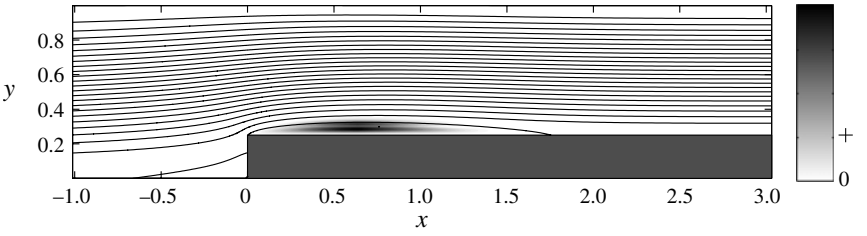


FIGURE 11. Receptivity to spatially localized feedback (2.16) for the most dangerous mode for $\Gamma = 0.25$ at $Re_c = 5888.4$.

globally most important effect is represented by I_2' (last row of table 3). The term I_2' describes the classical lift-up effect by which basic flow momentum is transported by the cross-stream perturbation velocity $\tilde{\boldsymbol{u}}_\perp \cdot \boldsymbol{\nabla} \boldsymbol{u}_0$, feeding back on the parallel component $\tilde{\boldsymbol{u}}_\parallel$. By comparing figure 7(*a*) with figure 7(*b*), one can hardly notice any difference between the sum of all energy-production rates $\sum I_i'$ and the sum of $I_2' + I_4'$.

To sum up, the physical nature of the instability is a combination of the lift-up mechanism and flow deceleration near the separating streamline of the secondary recirculating vortex, providing a feedback for the disturbances to be self-sustained.

3.4. *Sensitivity results*

A sensitivity analysis was also performed for $\Gamma = 0.25$ at critical conditions. From figure 10, it can be seen that the flow is most sensitive to initial conditions and momentum forcing just at the entrance of the channel extending forward to the step front. A certain receptivity is also found after the step within the secondary separation zone.

The product between the direct and the adjoint fields $\Upsilon = |\hat{\boldsymbol{u}}|\,|\hat{\mathbf{u}}|$ (2.16) is evaluated in figure 11, showing the regions where the leading eigenvalue and, consequently, the stability boundary is most sensitive to local perturbations. It can be seen that the highest effect on the growth rate and thus the stability boundary is provided by perturbations localized in the region of the secondary recirculating vortex. This result is consistent with the above energy analysis, which has also shown that the instability is caused by quite localized processes after the step and within the region of the secondary recirculating bubble.

Stüer *et al.* (1999) observed by hydrogen bubble visualization that the turbulent regime for $\Gamma = 0.25$ sets in at around $Re \approx 4800$. This difference of about $-20\,\%$ with respect to the global stability boundary may be related to sidewall effects and/or to

https://doi.org/10.1017/jfm.2012.28 Published online by Cambridge University Press

the sensitivity of the flow to oncoming perturbations, which both cannot be avoided in laboratory experiments.

4. Conclusions

The global linear stability of the flow past a forward-facing step has been considered for a quasicontinuous variation of the constriction ratio Γ. The influence of the grid resolution and of the in- and outlet channel lengths on the stability boundaries has been scrutinized to ensure independent results. The critical Reynolds number Re_c takes its maximum value for the smallest constriction ratio considered. Re_c decreases gradually as the step height is increased. By using an appropriate length scale, the scaled critical values Re_c^* and k_c^* approach a linear asymptotic regime for large step heights $(1 - \Gamma) \ll 1$. All three-dimensional critical modes are stationary and locally confined to the secondary recirculation bubble, which is thus identified as the main source of the instability. An *a posteriori* energy-transfer analysis showed that all instabilities can be explained in terms of the combined action of lift-up and flow deceleration.

The critical mode and its associated energy-production rates were visualized for $\Gamma = 0.25$. We found that the critical wavelength is approximately three times the step height, in agreement with the experimental and numerical results of Stüer *et al.* (1999) and Wilhelm *et al.* (2003). Almost all of the kinetic perturbation energy is produced near the separating streamline of the secondary vortex of the basic flow. The critical mode appears as steady, streaky structures downstream of the step corner. This streak formation has also been observed in the experiments of Pollard *et al.* (1996) and Stüer *et al.* (1999). The alternating slow and fast streaks of the perturbations are self-sustained here due to the feedback provided by the recirculating bubble. The sensitivity analysis for spatially localized perturbations likewise identified the secondary recirculating bubble to be extremely important for the temporal growth rate and thus for the stability boundary. It is worth mentioning that the topology of the critical mode is very similar to the one detected by Lanzerstorfer & Kuhlmann (2011) in the backward-facing step problem for small step heights.

A problem for the experimental observability of the global instability of the forward-facing step problem is the sensitivity of the flow with respect to oncoming disturbances, which was revealed by the absolute value of the adjoint of the critical mode. An open question is the existence of convective instabilities below the absolute stability boundaries as presented in the current work. Transient growth analyses in a global framework to be conducted in future studies may contribute to answer this question. Also, direct numerical simulations and experiments focusing on the global three-dimensionality would be of interest to assess the physical relevance of the global instability modes.

REFERENCES

ALBENSOEDER, S., KUHLMANN, H. C. & RATH, H. J. 2001 Three-dimensional centrifugal-flow instabilities in the lid-driven cavity problem. *Phys. Fluids* **13**, 121–135.

BARKLEY, D., GOMES, M. G. M. & HENDERSON, R. D. 2002 Three-dimensional instability in flow over a backward-facing step. *J. Fluid Mech.* **473**, 167–190.

CHIBA, K., ISHIDA, R. & NAKAMURA, K. 1995 Mechanism for entry flow instability through a forward-facing step channel. *J. Non-Newtonian Fluid Mech.* **57**, 271–282.

DENNIS, S. C. R. & SMITH, F. T. 1980 Steady flow through a channel with a symmetrical constriction in the form of a step. *Proc. R. Soc. Lond.* A **372**, 393–414.

https://doi.org/10.1017/jfm.2012.28 Published online by Cambridge University Press

GIANNETTI, F. & LUCHINI, P. 2007 Structural sensitivity of the first instability of the cylinder wake. *J. Fluid Mech.* **581**, 167–197.

LANDAHL, M. T. 1975 Wave breakdown and turbulence. *SIAM J. Appl. Math.* **28**, 735–756.

LANDAHL, M. T. 1980 A note on an algebraic instability of inviscid parallel shear flows. *J. Fluid Mech.* **98**, 243–251.

LANZERSTORFER, D. & KUHLMANN, H. C. 2011 Global stability of the two-dimensional flow over a backward-facing step. *J. Fluid Mech.* **693**, 1–27.

MARINO, L. & LUCHINI, P. 2009 Adjoint analysis of the flow over a forward-facing step. *Theor. Comput. Fluid Dyn.* **23**, 37–54.

PLOTKIN, A. & MEI, R. W. 1986 Navier–Stokes solutions for laminar incompressible flows in forward-facing step geometries. *AIAA J.* **24** (7), 1106–1111.

POLLARD, A., WAKARANI, N. & SHAW, J. 1996 Genesis and morphology of erosional shapes associated with turbulent flow over a forward-facing step. In *Coherent Flow Structures in Open Channels*, pp. 249–265. Wiley.

SCHMID, P. J. & HENNINGSON, D. S. 2001 *Stability and Transition in Shear Flows*. Springer.

STÜER, H. 1999 Investigation of separation on a forward facing step. PhD thesis, ETH Zürich.

STÜER, H., GYR, A. & KINZELBACH, W. 1999 Laminar separation on a forward facing step. *Eur. J. Mech.* B/*Fluids* **18**, 675–692.

THEOFILIS, V. 2000 Globally unstable basic flows in open cavities. In *6th AIAA/CEAS Aeroacoustics Conference. AIAA 2000-1965*.

THEOFILIS, V. 2003 Advances in global linear instability analysis of nonparallel and three-dimensional flows. *Prog. Aerosp. Sci.* **39**, 249–315.

THEOFILIS, V. 2011 Global linear instability. *Annu. Rev. Fluid Mech.* **43**, 319–352.

WILHELM, D. 2000 Numerical investigation of three-dimensional separation in a forward-facing step flow using a spectral element method. PhD thesis, ETH Zürich.

WILHELM, D., HÄRTEL, C. & KLEISER, L. 2003 Computational analysis of the two-dimensional–three-dimensional transition in forward-facing step flow. *J. Fluid Mech.* **489**, 1–27.

https://doi.org/10.1017/jfm.2012.28 Published online by Cambridge University Press